Stabilizing NMPC Approaches for Underactuated Mechanical Systems on the SE(3) Manifold⋆

Jean C. Pereira[a,∗], Valter J. S. Leite[a], Guilherme V. Raffo[b]

[a]*Department of Mechatronics Engineering,* Campus *Divinópolis — CEFET–MG, Divinópolis, MG, 35503-822, Brazil*
[b]*Department of Electronics Engineering, Federal University of Minas Gerais, Belo Horizonte, MG 31270-901, Brazil*

Abstract

This paper addresses the motion control problem for underactuated mechanical systems with full attitude control and one translational force input to manage the six degrees of freedom involved in the three-dimensional Euclidean space. These systems are often classified as second-order nonholonomic due to their completely nonintegrable acceleration constraints. To tackle this complex control problem, we propose two nonlinear model predictive control (NMPC) schemes that ensure closed-loop stability and recursive feasibility without terminal conditions. The system dynamics are modeled on the SE(3) manifold for a globally and unique description of rigid body configurations. One NMPC scheme also aims to reduce mission time as an economic criterion. The controllers' effectiveness is validated through numerical experiments on a quadrotor UAV.

Keywords: Underactuated mechanical systems; NMPC; Second-order nonholonomic systems; Dissipativity-based stability.

arXiv:2503.17458v1 [eess.SY] 21 Mar 2025

1. Introduction

Unmanned vehicles have gained significant attention recently due to their wide range of applications, including security, agriculture, infrastructure inspection, exploration, wildlife conservation, package delivery, and remote sensing (He et al., 2022; Penicka & Scaramuzza, 2022; Cenerini et al., 2023; Hamrah et al., 2018). Depending on their environment, these vehicles are categorized as Autonomous Ground Vehicles (AGVs), Autonomous Underwater Vehicles (AUVs), and Unmanned Aerial Vehicles (UAVs) (Liu et al., 2017; Heshmati-Alamdari et al., 2021; Hua et al., 2013). Typically, they are designed with fewer actuators than degrees of freedom (DOF) to reduce weight and cost, making them underactuated systems (He et al., 2022).

This work investigates the motion control of underactuated mechanical systems globally represented in the SE(3) manifold, which features full attitude control with a single translational input, using four independent control inputs to manage the six DOF in the three-dimensional Euclidean space. These systems are often classified as second-order nonholonomic due to their nonintegrable acceleration constraints. The Special Euclidean group SE(3) is defined as an ordered pair $(R, \xi) \in$ SE(3), where $R \in$ SO(3)[1] is a rotation matrix indi-

cating the body's attitude, and $\xi \in \mathbb{R}^3$ denotes the position of a point, typically the origin of the body-fixed frame, in the inertial frame (Lee et al., 2018). Minimal representations, like Euler-angle and angle-axis parametrizations, face singularities and are only locally effective (Lee, 2015). In contrast, unit quaternions are singularity-free (Casau et al., 2015) and provide a double cover of the attitude space, leading to potential inconsistencies such as the unwinding phenomenon (Mayhew et al., 2012). Thus, using rotation matrices and the SE(3) manifold is advantageous for controlling underactuated mechanical systems, particularly for aggressive motions, as this representation is unique and independent of local coordinates (Chaturvedi et al., 2011; He et al., 2022), effectively capturing the coupling between rotational and translational dynamics (Nikhilraj et al., 2019). A SE(3) manifold model applies to a wide range of rotary-wing aircraft, including helicopters (Frazzoli et al., 2000), multi-propeller helicopters (Hua et al., 2013), and ducted fans (Pflimlin et al., 2007), as well as satellites (Yoshimura et al., 2016). Accordingly, since the resultant force vector typically aligns with a body-fixed direction, the control of attitude and translational dynamics must be integrated simultaneously (Hamrah et al., 2018).

Stabilizing this class of underactuated mechanical systems is challenging, as nonholonomic systems with rotational DOF cannot be globally asymptotically stabilized at a constant equilibrium via continuous feedback (Brockett, 1983; Bhat & Bernstein, 2000). To address this, several solutions have been proposed, including discontinuous control laws on SE(3) (Fjellstad & Fossen, 1994; Egeland et al., 1996), time-varying quaternion continuous feedback (Pettersen & Egeland, 1999), and hybrid quaternion feedback strategies (Casau et al., 2015). However, these approaches disregard control input constraints, which are crucial in practical applications (Li & Yan, 2017).

[1]The notation SO abbreviates *special orthogonal*. Generally, the space of rotation matrices in $\mathbb{R}^{n \times n}$ is given by SO$(n) := \{R \in \mathbb{R}^{n \times n} : RR^\top = I, \det R = +1\}$ (Murray et al., 1994).

To address the challenges of controlling underactuated vehicles, model predictive control (MPC) schemes have been employed due to their capability to handle constrained multiple-input multiple-output nonlinear systems efficiently (Raffo et al., 2010; Kunz et al., 2013; Alexis et al., 2014; Li & Yan, 2017; Eskandarpour & Sharf, 2020; Liang et al., 2021; Cenerini et al., 2023; Nascimento et al., 2023). However, many studies have used local attitude parametrization, like Euler angles, and separated the problem into attitude and position control layers (Raffo et al., 2010; Alexis et al., 2014; Eskandarpour & Sharf, 2020), which can be limiting for tasks involving simultaneous position and attitude references. Addressing such limitation, Murilo & Lopes (2019) have introduced a unified NMPC framework using Euler angles for quadrotor UAVs, but it can also suffer from singularities and be limited to local effectiveness. Similarly, Wehbeh & Sharf (2022) have proposed a unified trajectory tracking scheme using time-dependent linearization on the Lie algebra of SO(3) to avoid singularities. Despite achieving applicable results, the control strategy's feasibility and closed-loop stability have not been demonstrated.

For simplified and linearized models, such as in Eskandarpour & Sharf (2020), feasibility and closed-loop stability analyses of MPC are typically provided. However, these analyses are limited for NMPC strategies considering a complete nonlinear model of underactuated vehicles without decoupling rotational and translational motions (Liang et al., 2021). Classical MPC with terminal constraints usually requires a locally continuous time-invariant state feedback controller for system stability (Mayne et al., 2000), but Brockett's theorem (Brockett, 1983) states that there is no such feedback controller for nonholonomic systems. To address this, Li & Yan (2017) have proposed an NMPC scheme using a transformed model with homogeneity properties for underactuated marine vehicles, although it requires changing the control law back. In Liang et al. (2021), an NMPC with terminal constraints developed using Lyapunov's stability theory and backstepping has been presented for marine vehicles in two-dimensional Euclidean space, introducing an auxiliary time-varying tracking controller. Another strategy to overcome the stability requirement is focusing on NMPC frameworks without terminal conditions.

MPC schemes without stabilizing constraints are easier to design, require less computational effort, and are commonly used in industrial applications compared to those with stabilizing constraints (Mehrez et al., 2020). Furthermore, they provide larger stability regions for a fixed prediction horizon (Grüne & Pannek, 2017). In this type of MPC, closed-loop stability is typically ensured by indirect techniques using bounds on the MPC value function to determine a stabilizing prediction horizon length (Tuna et al., 2006; Grüne et al., 2010), or through recent advancements in economic MPC (EMPC) that leverage conditions based on dissipativity and controllability properties (Grüne & Stieler, 2014). In EMPC, the controller's primary goal is not to stabilize a precomputed trajectory or steady state but to optimize performance based on economic cost criteria, such as minimizing energy or time (Grüne & Pirkelmann, 2020).

This work addresses the motion control problem of a class of underactuated mechanical systems in the non-Euclidean space SE(3). The closed-loop stability analysis relies on dissipativity properties typically associated with EMPC frameworks. Therefore, we propose two NMPC schemes without terminal conditions to tackle the stabilization problem on the SE(3) manifold. The first scheme regulates the vehicle's pose to achieve a desired equilibrium point, while the second incorporates mission time as an economic criterion, retaining the features of the first controller. This approach utilizes an exponential weight in the stage cost to indirectly achieve time-optimality, adapting the fixed horizon strategy proposed by Verschueren et al. (2017).

The contributions of the paper are threefold: i) the development of NMPC schemes for the stabilization of a class of underactuated mechanical systems with second-order nonholonomic constraints globally represented on the SE(3) manifold, capable of addressing constraints on inputs and states; ii) guarantees of closed-loop stability and recursive feasibility for both schemes, derived from a dissipativity-based analysis that extends established principles (Tuna et al. (2006); Grüne et al. (2010); Grüne & Stieler (2014); Grüne & Pannek (2017)) to second-order nonholonomic systems on the SE(3) manifold, where unique challenges arise from state-space representation and constraints; and iii) the introduction of an NMPC scheme that considers mission time reduction as an economic criterion, which is particularly significant for practical applications like UAV navigation and robot motion, where operational efficiency is critical.

Notations

$\mathbb{R}$, $\mathbb{R}^n$, $\mathbb{R}^{m \times n}$, and $\mathbb{R}_0^+$ denote the spaces of real numbers, vectors with n real entries, matrices of dimension $m \times n$ with real entries, and the non-negative real numbers, respectively. The identity matrix is represented by I_n, while zero matrices are denoted by $\mathbf{0}_{m \times n}$ and quadratic zero matrices by $\mathbf{0}_n$. The transpose of a matrix M is $M^\top$, and for a square matrix, the transpose of its inverse is $M^{-\top}$. The set of integers from 0 to i is denoted by $\mathbb{I}_{0:i}$. A continuous function $\alpha : \mathbb{R}_0^+ \to \mathbb{R}_0^+$ is a class $\mathcal{K}$ function if it is zero at zero and strictly monotonically increasing; it is a class $\mathcal{K}_\infty$ function if unbounded. A continuous function $\beta : \mathbb{R}_0^+ \times \mathbb{R}_0^+ \to \mathbb{R}_0^+$ is a $\mathcal{KL}$-function if $\beta(\cdot, t) \in \mathcal{K}$ for all $t \in \mathbb{R}_0^+$ and $\beta(r, \cdot)$ strictly monotonically decays to zero for each $r > 0$. The vector space of skew matrices is denoted by $\mathfrak{so}(\cdot)$, and $\mathcal{S}(\cdot)$ represents the skew-symmetric matrix operator. Time dependence of a variable v is denoted by $v(t)$ or $v(k)$ for clarity.

2. Problem Formulation

Consider a finite-dimensional nonlinear system of the form

$$\dot{x}(t) = g(x(t), u(t)), \tag{1}$$

for some state-transition map $g : X \times U \to X$, with X and U being the state and control normed spaces, respectively. Additionally, $x \in \mathbb{X} \subseteq X$ represents the states and $u \in \mathbb{U} \subseteq U$ the inputs, with $\mathbb{X}$ and $\mathbb{U}$ designating, respectively, the set of admissible states and inputs.

By considering a nonlinear discrete-time invariant model obtained from (1)

$$x(j + 1) = g_d(x(j), u(j)), \qquad (2)$$

with $t = jT_s$, where T_s is the sampling time, the discrete-time optimal control problem (OCP) to be solved at each time instant k, with $t = kT_s$, is posed as

$$
\begin{aligned}
\min_{x,u} \quad & \sum_{j=0}^{N_p} \ell(x(k+j), u(k+j)) \\
\text{s.t.} \quad & x(j+1) = g_d(x(j), u(j)), \quad x_0 = x(k), \\
& x \in \mathbb{X}, \qquad\qquad\qquad \forall j \in \mathbb{N}_p, \\
& u \in \mathbb{U}, \qquad\qquad\qquad \forall j \in \mathbb{N}_p,
\end{aligned}
\qquad (3)
$$

where $\ell : X \times U \to \mathbb{R}_0^+$ is the stage cost, x_0 is the current state, and $\mathbb{N}_p$ represents the non-negative integers bounded by the prediction horizon N_p. The optimization variables are given by the sequences $x := (x(0), x(1), \ldots, x(N_p))$ and $u := (u(0), u(1), \ldots, u(N_p - 1))$.

The following MPC iteration defines the feedback law at each time instant k: i) Measure the current state x_0; ii) Solve the OCP (3) to obtain the optimal control sequence $u^\star$; iii) Apply the first control action $u^\star(0)$ until the next time instant.

Definition 1 (adapted from Grüne & Stieler (2014)). *A pair $(x^e, u^e) \in \mathbb{X} \times \mathbb{U}$ is called equilibrium for the control system (1) if it satisfies the condition $g_d(x^e, u^e) = x^e$. An equilibrium is optimal if it solves the optimization problem*

$$\min_{x \in \mathbb{X}, u \in \mathbb{U}} \ell(x, u) \quad s.t. \ g_d(x, u) - x = 0 . \qquad (4)$$

Therefore, for the class of underactuated mechanical systems with second-order nonholonomic constraints, with the state-transition map g defined by (5)-(8), the following problems are addressed:

Problem 1. *Steer the underactuated mechanical system to a desired set-point x^e, which is an optimal equilibrium for the control system.*

Problem 2. *Solve Problem 1 regarding the mission time as an economic criterion.*

3. Preliminaries

3.1. Dynamics of a class of underactuated mechanical systems on SE(3)

The system is modeled as an underactuated rigid body with a frame $\mathcal{B} = \{B_1, B_2, B_3\}$ attached to it. The inertial frame $\mathcal{I} = \{I_1, I_2, I_3\}$ is fixed with respect to the Earth. The configuration manifold is represented by the ordered pair $(R_{\mathcal{B}}^{\mathcal{I}}, \xi^{\mathcal{I}}) \in$ SE(3), where the rotation matrix $R_{\mathcal{B}}^{\mathcal{I}} \in$ SO(3) describes the rigid body attitude, and $\xi^{\mathcal{I}} \in \mathbb{R}^3$ denotes the center of mass position of the vehicle. The state space of the system is TSE(3), the tangent bundle of SE(3), allowing the motion dynamics to be represented through the states $x := (R_{\mathcal{B}}^{\mathcal{I}}, \xi^{\mathcal{I}}, \omega^{\mathcal{B}}, v^{\mathcal{I}}) \in$ TSE(3). The continuous-time equations of motion are given by (Kobilarov, 2013)

$$\dot{\xi}^{\mathcal{I}} = v^{\mathcal{I}}, \qquad (5)$$

$$m\dot{v}^{\mathcal{I}} = f^{\mathcal{I}} = R_{\mathcal{B}}^{\mathcal{I}} e^{\mathcal{B}} T + f_e^{\mathcal{I}}(\xi^{\mathcal{I}}, v^{\mathcal{I}}), \qquad (6)$$

$$\dot{R}_{\mathcal{B}}^{\mathcal{I}} = R_{\mathcal{B}}^{\mathcal{I}} S(\omega^{\mathcal{B}}), \qquad (7)$$

$$J^{\mathcal{B}} \dot{\omega}^{\mathcal{B}} = -\omega^{\mathcal{B}} \times J^{\mathcal{B}} \omega^{\mathcal{B}} + \tau^{\mathcal{B}} + \tau_e^{\mathcal{B}}(x), \qquad (8)$$

where $T \in \mathbb{R}$ is a control force applied in a body-fixed direction defined by the unit vector $e^{\mathcal{B}} \in \mathbb{R}^3$, $\tau^{\mathcal{B}} \in \mathbb{R}^3$ is the control torque expressed in $\mathcal{B}$, both applied at the motion system center of mass, $v^{\mathcal{I}} \in \mathbb{R}^3$ is the center of mass linear velocity expressed in $\mathcal{I}$, $\omega^{\mathcal{B}} \in \mathbb{R}^3$ is the angular velocity of the body with respect to $\mathcal{I}$, expressed in $\mathcal{B}$, $S(\omega^{\mathcal{B}}) \in \mathfrak{so}(3)$, m is the total mass of the system, and $J^{\mathcal{B}}$ is the inertia tensor. The vehicle is subjected to known external forces and torques given by the functions $f_e^{\mathcal{I}} : \mathbb{R}^3 \times \mathbb{R}^3 \to \mathbb{R}^3$ and $\tau_e^{\mathcal{B}} :$ TSE(3) $\to \mathbb{R}^3$, respectively.

3.2. Attitude error function on SO(3)

Although a system modeled by a rotation matrix $R \in$ SO(3) has no representational singularities, selecting a positive definite error function to measure the difference between configurations is crucial for the control design. Consider the i-th configuration error function $\Psi_i(R, R_d) = \frac{1}{2}\|Re_i - R_d e_i\|^2 = 1 - Re_i \cdot R_d e_i$, where $e_i \in \mathsf{S}^2 := \{q \in \mathbb{R}^3 : \|q\|^2 = 1\}$ is a unit-vector starting from the mass center of the rigid body (Lee, 2015). Let e_1 and e_2 be orthogonal vectors. For positive constants $k_i > 0$, the complete configuration error function is given by

$$\Psi(R, R_d) = k_1 \Psi_1(R) + k_2 \Psi_2(R). \qquad (9)$$

It can be noticed that $\Psi_i(R, R_d)$ represents the geometric projection between Re_i and $R_d e_i$, and $\Psi_i(R, R_d)$ is positive definite about $Re_i = R_d e_i$. Therefore, the complete configuration error $\Psi(R, R_d)$, given by (9), is positive definite about $R = R_d$, that is, $\Psi(R, R_d) > 0$ for all $R \neq R_d$, and $\Psi(R, R_d) = 0$ if only if $R = R_d$.

3.3. System discretization

The Euler method is used to discretize the dynamic equations (5) and (6), with the predicted time $t_p = jT_s$, resulting in

$$\xi^{\mathcal{I}}(j + 1) = \xi^{\mathcal{I}}(j) + T_s v^{\mathcal{I}}(j), \qquad (10)$$

$$v^{\mathcal{I}}(j + 1) = v^{\mathcal{I}}(j) + T_s \left(\frac{R_{\mathcal{B}}^{\mathcal{I}}(j) e^{\mathcal{B}} T(j) + f_e^{\mathcal{I}}(j)}{m} \right). \qquad (11)$$

The traditional Euler method does not ensure that the predicted $R_{\mathcal{B}}^{\mathcal{I}}(j + 1)$ remains on SO(3). Consequently, specific geometric integration methods have been developed for numerically integrating (7) and (8) (Ortolan, 2011). These methods primarily rely on the geometric relationship between SO(3) and $\mathfrak{so}(3)$, with $\mathfrak{so}(3)$ representing the tangent space of SO(3) at the identity $I_3 \in$ SO(3). Since $\mathfrak{so}(3)$ is the Lie algebra of the Lie Group SO(3), the map $\mathfrak{so}(3) \to$ SO(3) corresponds to the exponential matrix map. Thus, the solution to the differential equation (7) is given by the exponential map $R_{\mathcal{B}}^{\mathcal{I}}(t) = e^{tS(\omega^{\mathcal{B}}(t))} = I_3 + tS(\omega^{\mathcal{B}}(t)) + \frac{(tS(\omega^{\mathcal{B}}(t)))^2}{2!} + \ldots$, which can be discretized as $R_{\mathcal{B}}^{\mathcal{I}}(j) = R_{\mathcal{B}}^{\mathcal{I}}(jT_s) = e^{jT_s S(\omega^{\mathcal{B}}(jT_s))}$. Thus, given the current configuration at the j-th sample time $(R_{\mathcal{B}}^{\mathcal{I}}(j), \omega^{\mathcal{B}}(j))$, the next configuration $(R_{\mathcal{B}}^{\mathcal{I}}(j+1), \omega^{\mathcal{B}}(j+1))$ is defined by the following iteration rule (Simo & Vu-Quoc, 1988):

$$\omega^{\mathcal{B}}(\bar{j}) = \omega^{\mathcal{B}}(j) + \frac{T_s}{2}(J^{\mathcal{B}})^{-1}\alpha(j), \qquad (12)$$

$$R_{\mathcal{B}}^{\mathcal{I}}(j+1) = R_{\mathcal{B}}^{\mathcal{I}}(j)\mathrm{cay}(T_s\omega^{\mathcal{B}}(\bar{j})), \tag{13}$$

$$\omega^{\mathcal{B}}(j+1) = \omega^{\mathcal{B}}(\bar{j}) + \frac{T_s}{2}(J^{\mathcal{B}})^{-1}\alpha(j), \tag{14}$$

where $\alpha(j) = J^{\mathcal{B}}\omega^{\mathcal{B}}(j) \times \omega^{\mathcal{B}}(j) + \tau^{\mathcal{B}}(j) + \tau_e^{\mathcal{B}}(j)$, and $\mathrm{cay}(\cdot)$ is the Cayley map, which is the second-order approximation of the matrix exponential function defined by $\mathrm{cay}(v) := (I_3 + \frac{1}{2}\mathcal{S}(v))(I_3 - \frac{1}{2}\mathcal{S}(v))^{-1} \approx \mathrm{expm}(\mathcal{S}(v))$.

3.4. MPC Stability Based on Strict Dissipativity

The main dissipativity-based stability result for MPC schemes without terminal conditions presented in Grüne & Stieler (2014) is revisited in this section (see also Grüne & Pannek (2017) for further details).

Definition 2. *Consider $x^e \in \mathbb{X}$ to be an equilibrium for the closed-loop system. The equilibrium is said to be practically asymptotically stable w.r.t. $\rho \geq 0$ on a set $S \subseteq \mathbb{X}$ with $x^e \in S$ if there exists $\beta \in \mathcal{KL}$ such that*

$$\|x - x^e\| \leq \max\{\beta(\|x_0 - x^e\|, k), \rho\} \tag{15}$$

holds for all $x_0 \in S$ and all $k \in \mathbb{N}$. The equilibrium is globally practically asymptotically stable w.r.t. $\rho \geq 0$ if (15) holds on $S = \mathbb{X}$.

Assumption 1. *The OCP (3) is strictly dissipative with respect to the equilibrium $(x^e, u^e) \in \mathbb{X} \times \mathbb{U}$, that is, there is a non-negative storage function $\lambda : \mathbb{X} \to \mathbb{R}_0^+$, and a function $\alpha_\ell \in \mathcal{K}_\infty$ such that*

$$\lambda(g_d(x,u)) - \lambda(x) \leq \ell(x,u) - \ell(x^e, u^e) - \alpha_\ell(\|x - x^e\|), \tag{16}$$

holds for all $x \in \mathbb{X}$, $u \in \mathbb{U}$, $j \in \mathbb{N}$.

Assumption 2. *The state and control constraint set $\mathbb{X}$ and $\mathbb{U}$ are compact, the functions g_d, ℓ and λ are continuous, and λ is Lipschitz continuous on a ball $\mathcal{B}_\epsilon(x^e) := \{x \in \mathbb{X} | \|x - x^e\| < \epsilon\}$ for $\epsilon > 0$.*

Assumption 3. *The system (2) is local controllable on $\mathcal{B}_\epsilon(x^e)$, that is, there is $\epsilon > 0$, $N' \in \mathbb{N}$, $C > 0$ such that $\forall x_0 \in \mathcal{B}_\epsilon(x^e)$ $\exists u_1 \in \mathbb{U}^{N'}(x_0)$, $\exists u_2 \in \mathbb{U}^{N'}(x^e)$ with $x_{u_1}(N', x_0) = x^e$ and $x_{u_2}(N', x^e) = x_0$, where $x_{u_i}(N', x_0)$ denotes the solution of (2) for a control sequence $u_i \in \mathbb{U}^{N'}(x_0)$ emanating from the initial value $x_0 \in \mathbb{X}$, and $\mathbb{U}^{N'} x_0)$ represents the set of all admissible control sequences which holds both $u \in \mathbb{U}$ and $x_u(j, x_0) \in \mathbb{X}$ $\forall j \in \mathbb{I}_{0:N'}$. Moreover, $\max\{\|x_{u_1}(N', x_0) - x^e\|, \|x_{u_2}(N', x^e) - x_0\|, \|u_1 - u^e\|, \|u_2 - u^e\|\} \leq C\|x_0 - x^e\|$ $\forall j \in \mathbb{I}_{0:N'-1}$.*

Assumption 4. *The system (2) is finite time controllable into $\mathcal{B}_\epsilon(x^e)$, that is, for $\epsilon > 0$ from Assumption 3 there is $N' \in \mathbb{N}$ such that for each $x_0 \in \mathbb{X}$ there is $j \leq N'$ and $\mathbb{U}^{N'}(x_0)$ with $x_u(j, x_0) \in \mathcal{B}_\epsilon(x^e)$.*

Theorem 1 (Adapted from Grüne & Stieler (2014)).

Consider the economic MPC problem without terminal conditions arising from the receding horizon solution to OCP (3) satisfying Assumptions 1-4. Then, there exists a sufficiently large horizon $N_p \in \mathbb{N}$, such that the closed-loop system defined by (2) is practically asymptotically stable w.r.t ϵ, where $\epsilon \to 0$ as $N_p \to \infty$.

Proposition 1 (Adapted from Grüne & Pannek (2017)). *Let Assumptions 1-4 hold. If, for the horizon $N_p \in \mathbb{N}$, the OCP (3) is feasible for $j = 0$ and $x_0 \in \mathbb{X}$, then it is feasible for all $j \in \mathbb{N}$.*

4. Nonlinear Model Predictive Control Schemes

This section describes the proposed control strategies for motion control a class of underactuated mechanical systems with second-order nonholonomic constraints modeled on $\mathsf{SE}(3)$. Both schemes regulate the vehicle to a desired equilibrium and use an attitude error function defined on $\mathsf{SO}(3)$. The fundamental difference between these two NMPC schemes is that the second formulation incorporates mission time as an economic criterion, whereas the first one does not.

4.1. NMPC for motion control of a class of underactuated mechanical systems on $\mathsf{SE}(3)$

Considering the discrete-time system g_d given by (10)-(14), the NMPC scheme repeatedly solves, in each sample time k, the following optimal control problem:

$$\min_{x,u} \sum_{j=0}^{N_p} \|\bar{x}(k+j)\|_{Q_{\bar{x}}}^2 + \|\bar{u}(k+j)\|_{Q_{\bar{u}}}^2$$
$$\text{s.t.} \quad x(j+1) = g_d(x(j), u(j)), \quad x_0 = x(k), \tag{17}$$
$$x \in \mathbb{X}, \qquad\qquad \forall j \in \mathbb{N}_p,$$
$$u \in \mathbb{U}, \qquad\qquad \forall j \in \mathbb{N}_p,$$

where $\bar{x} := \begin{bmatrix} (\xi^{\mathcal{I}})^\top & (v^{\mathcal{I}})^\top & \Psi(R_{\mathcal{B}}^{\mathcal{I}}, R_d) & (\omega^{\mathcal{B}})^\top \end{bmatrix}^\top \in \mathbb{R}^{10}$ and $\bar{u} := \begin{bmatrix} \|f^{\mathcal{I}}\| & (\tau^{\mathcal{B}})^\top \end{bmatrix}^\top \in \mathbb{R}^4$, with $Q_{\bar{x}} > 0$ being defined such that $\|\bar{x}\|_{Q_{\bar{x}}}^2 = k_p\|\xi^{\mathcal{I}}\|^2 + k_v\|v^{\mathcal{I}}\|^2 + k_\omega\|\omega^{\mathcal{B}}\|^2 + k_R\Psi^2(R_{\mathcal{B}}^{\mathcal{I}})$, and $Q_{\bar{u}} > 0$ being defined such that $\|\bar{u}\|_{Q_{\bar{u}}}^2 = k_f\|f^{\mathcal{I}}\|^2 + k_\tau\|\tau^{\mathcal{B}}\|^2$.

Remark 1. *Without loss of generality, the position equilibrium is set at the origin, $(\xi^{\mathcal{I}})^e = \begin{bmatrix} 0 & 0 & 0 \end{bmatrix}^\top$, and the equilibrium points for R_d, $v_d^{\mathcal{I}}$, and $\omega_d^{\mathcal{B}}$ are defined based on the system characteristics. Therefore, at equilibrium, $\ell(\bar{x}^e, \bar{u}^e) = 0$.*

4.2. NMPC for fast motion control of a class of underactuated mechanical systems on $\mathsf{SE}(3)$

Considering the discrete-time system, g_d, given by (10)-(14), the economic NMPC scheme repeatedly solves, in each sample time k, the following optimal control problem:

$$\min_{x,u} \sum_{j=0}^{N_p} \zeta^j \|\bar{x}(k+j)\|_{Q_{\bar{x}}}^2 + \|\bar{u}(k+j)\|_{Q_{\bar{u}}}^2$$
$$\text{s.t.} \quad x(j+1) = g_d(x(j), u(j)), \quad x_0 = x(k), \tag{18}$$
$$x \in \mathbb{X}, \qquad\qquad \forall j \in \mathbb{N}_p,$$
$$u \in \mathbb{U}, \qquad\qquad \forall j \in \mathbb{N}_p,$$

where $\zeta > 1$ is an exponential weight in the stage cost to induce rapid convergence to equilibrium (Verschueren et al., 2017), while the other variables are defined as in the previous NMPC formulation. It is noteworthy that the only difference between the OCPs (17) and (18) is the exponential weight, ζ.

Remark 2. *According to Theorem 1 of Verschueren et al. (2017), if N_p is greater than or equal to the time-optimal solution, there exists a number ζ_1 such that for all $\zeta > \zeta_1$, the solution of (18) becomes time-optimal. However, since the time-optimality in motion control problems mainly depends on the distance the vehicle must travel, which can be considerable, this work does not focus on the time-optimal solution. As a result, ζ is used as a tuning gain to promote faster motion.*

5. Feasibility and Stability Analysis

This section provides theoretical results ensuring the proposed controllers' closed-loop stability and recursive feasibility.

5.1. NMPC for motion control of a class of underactuated mechanical systems on SE(3)

Underactuated motion systems with second-order nonholonomic constraints represented by (5)-(8) are not linearly controllable by a continuous time-invariant feedback control law due to second-order nonholonomic constraints (Brockett, 1983), making the conventional Kalman rank condition (Kalman et al., 1963) unsuitable for assessing controllability. Instead, the N-controllability of the system is verified (Ferramosca et al., 2014).

Definition 3. *A linearized discrete-time system defined by matrices A and B is said to be N-step controllable if the N-controllability matrix $C_{o_N} := \begin{bmatrix} A^{N-1}B & \cdots & AB & B \end{bmatrix}$ has rank greater than or equal to the dimension of the system state vector $x \in \mathbb{R}^n$, i.e., $rank(C_{o_N}) \geq n$. This means that there exists a sequence $\{u(0), u(1), \cdots, u(N-1)\}$ that can transfer the system from any x_0 to x^e in N steps.*

Lemma 1. *The system (5)-(8) is four step controllable.*

Proof 1. *Due to the state variable $R_{\mathcal{B}}^{\mathcal{I}} \in$ SO(3), the conventional Jacobian linearization method cannot be used. Thus, from the exponential map of SO(3) and the isomorphism between $\mathfrak{so}(3)$ and $\mathbb{R}^3$, the infinitesimal variation principle of the rotational motion is applied, satisfying (Lee et al., 2018)*

$$\delta R_{\mathcal{B}}^{\mathcal{I}} = R_{\mathcal{B}}^{\mathcal{I}} \mathcal{S}(\eta), \tag{19}$$

$$\delta \omega^{\mathcal{B}} = \mathcal{S}(\omega^{\mathcal{B}})\eta + \dot{\eta}, \tag{20}$$

where a differentiable curve, $\eta \in \mathbb{R}^3$, is used to represent $\delta R_{\mathcal{B}}^{\mathcal{I}}$. Thus, the linearized equations of (5)-(8) in TSE(3) can be formulated as

$$\dot{\delta x} = A\delta x + B\delta u, \tag{21}$$

where $\delta x := \begin{bmatrix} (\delta \xi^{\mathcal{I}})^\top & (\delta v^{\mathcal{I}})^\top & \eta^\top & (\delta \omega^{\mathcal{B}})^\top \end{bmatrix}^\top \in \mathbb{R}^{12}$, and $\delta u := \begin{bmatrix} \delta T & (\delta \tau^{\mathcal{B}})^\top \end{bmatrix}^\top \in \mathbb{R}^4$. The matrices $A \in \mathbb{R}^{12 \times 12}$ and $B \in \mathbb{R}^{12 \times 4}$ are computed as

$$A = \begin{bmatrix} \mathbf{0}_3 & I_3 & \mathbf{0}_3 & \mathbf{0}_3 \\ \mathbf{0}_3 & \mathbf{0}_3 & -\frac{T}{m}R_{\mathcal{B}}^{\mathcal{I}}\mathcal{S}(e^{\mathcal{B}}) & \mathbf{0}_3 \\ \mathbf{0}_3 & \mathbf{0}_3 & -\mathcal{S}(\omega^{\mathcal{B}}) & I_3 \\ \mathbf{0}_3 & \mathbf{0}_3 & \mathbf{0}_3 & J^{-1}(\mathcal{S}(J\omega^{\mathcal{B}}) - \mathcal{S}(\omega^{\mathcal{B}})J) \end{bmatrix},$$

$$B = \begin{bmatrix} \mathbf{0}_{3 \times 1} & \mathbf{0}_3 \\ \frac{1}{m}R_{\mathcal{B}}^{\mathcal{I}}e^{\mathcal{B}} & \mathbf{0}_3 \\ \mathbf{0}_{3 \times 1} & \mathbf{0}_3 \\ \mathbf{0}_{3 \times 1} & J^{-1} \end{bmatrix}.$$

It can be verified that, considering $N = 4$, $rank\left(\begin{bmatrix} A^3B & A^2B & AB & B \end{bmatrix}\right) = 12$, which is equal to the dimension of the state vector δx. Therefore, the system (5)-(8) is four step controllable.

Remark 3. *Since the dynamics of the system (5)-(8) are sufficiently smooth, Lemma 1 ensures local controllability within a ball $\mathcal{B}_\epsilon(x_i^e) := \{x \in \mathbb{X} \mid \|x - x_i^e\| < \epsilon\}$ for $\epsilon > 0$. Additionally, as the proposed linearized model (21) is continuous in TSE(3), it can be defined for any $x_i^e \in$ TSE(3). Thus, for a desirable equilibrium x_d^e defining the ball $\mathcal{B}_\epsilon(x_d^e)$, for each $x_0 \in \mathbb{X}$, a finite sequence of κ intermediate targets $x_i^e \in \mathbb{X}$ exists, for $i = 1, \ldots, \kappa$, with $x(j) \in \mathcal{B}_\epsilon(x_{k-1}^e) \cap \mathcal{B}_\epsilon(x_k^e)$, $x_\kappa^e \in \mathcal{B}_\epsilon(x_d^e)$, where $4 \leq j \leq N' \in \mathbb{N}$. This sequence ensures that the trajectory starting from $x_0 \in \mathbb{X}$, denoted $x_u(j, x_0)$, passes through $\mathcal{B}_\epsilon(x_i^e) \cap \mathcal{B}_\epsilon(x_{i+1}^e) \cap \cdots \cap \mathcal{B}_\epsilon(x_d^e)$. Therefore, the system is finite-time controllable into $\mathcal{B}\epsilon(x_d^e)$.*

Lemma 2. *For sampling periods within the interval $0 < T_s < 1s$, if $k_v k_f \geq 0.25$ and $k_\omega k_\tau \geq 0.25$, then the OCP (17) is strictly dissipative with respect to the equilibrium $(\bar{x}^e, \bar{u}^e) \in \mathbb{X} \times \mathbb{U}$.*

Proof 2. *Consider the continuous time storage function candidate $\lambda :$ TSE(3) $\to \mathbb{R}$, defined as*

$$\lambda(x) = \frac{1}{2}(\omega^{\mathcal{B}})^\top J\omega^{\mathcal{B}} + \frac{1}{2}\|v^{\mathcal{I}}\|^2 - \mathcal{P}(R_{\mathcal{B}}^{\mathcal{I}}, \xi^{\mathcal{I}}), \tag{22}$$

which is the Lagrangian of the system on TSE(3), where $\mathcal{P}(R_{\mathcal{B}}^{\mathcal{I}}, \xi^{\mathcal{I}})$ is the potential energy that depends on the configuration $(R_{\mathcal{B}}^{\mathcal{I}}, \xi^{\mathcal{I}}) \in$ SE(3). It can be shown that for a rigid body rotating and translating in three dimensions under constant external forces and torques, the derivative of (22) represents the mechanical power of the system, given by

$$\frac{d}{dt}(\lambda(x)) = (\omega^{\mathcal{B}})^\top \tau^{\mathcal{B}} + (v^{\mathcal{I}})^\top f^{\mathcal{I}}. \tag{23}$$

In addition, for sampling periods within the interval $0 < T_s < 1s$, $\frac{d}{dt}(\lambda(x)) > \lambda(g_d(x, u)) - \lambda(x)$. Then, the right hand side of (16) can be overbounded by $\frac{d}{dt}(\lambda(x))$ yielding

$$\frac{d}{dt}\lambda(x) \leq \ell(x, u) - \ell(x^e, u^e) - \alpha_\ell(\|x - x^e\|). \tag{24}$$

Thus, for $\ell(x, u)$ defined by OCP (17), with $\ell(\bar{x}^e, \bar{u}^e) = 0$, and considering (23), the inequality (24) becomes

$$(\omega^{\mathcal{B}})^\top \tau^{\mathcal{B}} + (v^{\mathcal{I}})^\top f^{\mathcal{I}} \leq \|\bar{x}\|_{Q_{\bar{x}}}^2 + \|\bar{u}\|_{Q_{\bar{u}}}^2 - \alpha_\ell(\|\bar{x} - \bar{x}^e\|). \tag{25}$$

The inequality (25) is equivalent to

$$h_1(x) + h_2(x) \leq k_p\|\xi^{\mathcal{I}}\|^2 + k_R(\Psi(R_{\mathcal{B}}^{\mathcal{I}}))^2 - \alpha_\ell(\|\bar{x} - \bar{x}^e\|), \tag{26}$$

where $h_1(x) = (v^{\mathcal{I}})^\top f^{\mathcal{I}} - k_v\|v^{\mathcal{I}}\|^2 - k_f\|f^{\mathcal{I}}\|^2$ and $h_2(x) = (\omega^{\mathcal{B}})^\top \tau^{\mathcal{B}} - k_\omega\|\omega^{\mathcal{B}}\|^2 - k_\tau\|\tau^{\mathcal{B}}\|^2$.

For convenience, (26) will be analyzed by parts. First, by using the basic concept of quadratic difference between two real numbers, yields $\left(\sqrt{k_v}\|v^{\mathcal{I}}\| - \sqrt{k_f}\|f^{\mathcal{I}}\|\right)^2 \geq 0$, which can

5

be rewritten as $2\sqrt{k_v k_f}\|v^{\mathcal{I}}\|\|f^{\mathcal{I}}\| - k_v\|v^{\mathcal{I}}\|^2 - k_f\|f^{\mathcal{I}}\|^2 \leq 0$. Additionally, the Cauchy-Schwarz inequality give us $(v^{\mathcal{I}})^\top f^{\mathcal{I}} \leq \|v^{\mathcal{I}}\|\|f^{\mathcal{I}}\|$. Thus, if $k_v k_f \geq 0.25$, then

$$(v^{\mathcal{I}})^\top f^{\mathcal{I}} \leq k_v\|v^{\mathcal{I}}\|^2 + k_f\|f^{\mathcal{I}}\|^2 \implies h_1(x) \leq 0 \ \forall \ x \in \text{TSE(3)}. \quad (27)$$

Second, by following a similar approach, it can be verified that, for $k_\omega k_\tau \geq 0.25$, $h_2(x) \leq 0 \ \forall \ x \in TSE(3)$. Thus, $h_1(x) + h_2(x) \leq 0 \ \forall \ x \in \text{TSE(3)}$. Finally, if $k_v k_f \geq 0.25$, $k_\omega k_\tau \geq 0.25$, and since there exists a function $\alpha_\ell \in \mathcal{K}_\infty$ such that $k_p\|\xi^{\mathcal{I}}\|^2 + k_R(\Psi(R_{\mathcal{B}}^{\mathcal{I}}))^2 \geq \alpha_\ell(\|\bar{x} - \bar{x}^e\|)$, then, the inequality (26) holds, and, therefore, the OCP (17) is strictly dissipative with respect to the equilibrium (x^e, u^e).

The following theorem, based on the main dissipativity-based stability result for MPC schemes without terminal conditions by Grüne & Stieler (2014), establishes a minimum stabilizing horizon for the OCP (17).

Theorem 2. *The NMPC scheme defined by the OCP (17) is practically asymptotically stable for a sufficiently large horizon $N_p \in \mathcal{N} := \{n_p \in \mathbb{N} : n_p \geq 4\}$.*

Proof 3. *Lemmas 1 and 2 ensure that Assumptions 1-4 are satisfied. Then, Theorem 1 can be applied, and the NMPC scheme defined by the OCP (17) is practically asymptotically stable for a sufficiently large horizon $N_p \in \mathcal{N} := \{n_p \in \mathbb{N} : n_p \geq 4\}$.*

Proposition 2. *Assuming that, for horizon $N_p \in \mathcal{N}$, the OCP (17) is feasible for $k = 0$, then it is recursively feasible, i.e., it is feasible for all $k \in \mathbb{N}$.*

Proof 4. *The recursive feasibility follows from Proposition 1.*

5.2. NMPC for fast motion control of a class of underactuated mechanical systems on SE(3)

This subsection evaluates the closed-loop stability and recursive feasibility of the NMPC scheme described in Section 4.2. First, the following lemma specifies the conditions under which the OCP (18) is strictly dissipative.

Lemma 3. *For sampling periods within the interval $0 < T_s < 1s$, if $k_v k_f \geq 0.25$ and $k_\omega k_\tau \geq 0.25$, then the OCP (18) is strictly dissipative with respect to the equilibrium $(\bar{x}^e, \bar{u}^e) \in \mathbb{X} \times \mathbb{U}$.*

Proof 5. *Consider (22) as a continuous time storage function candidate. The dissipation inequality (24) considering the continuous time version of OCP (18) yields*

$$(\omega^{\mathcal{B}})^\top \tau^{\mathcal{B}} + (v^{\mathcal{I}})^\top f^{\mathcal{I}} \leq \zeta^t\|\bar{x}\|_{Q_{\bar{x}}}^2 + \|\bar{u}\|_{Q_{\bar{u}}}^2 - \alpha_\ell(\|\bar{x} - \bar{x}^e\|). \quad (28)$$

The inequality (28) can be rewritten as

$$h_3(x) + h_4(x) \leq \zeta^t(k_p\|\xi^{\mathcal{I}}\|^2 + k_R(\Psi(R_{\mathcal{B}}^{\mathcal{I}}))^2) - \alpha_\ell(\|\bar{x} - \bar{x}^e\|), \quad (29)$$

where $h_3(x) = (v^{\mathcal{I}})^\top f^{\mathcal{I}} - \zeta^t k_v\|v^{\mathcal{I}}\|^2 - k_f\|f^{\mathcal{I}}\|^2$ and $h_4(x) = (\omega^{\mathcal{B}})^\top \tau^{\mathcal{B}} - \zeta^t k_\omega\|\omega^{\mathcal{B}}\|^2 - k_\tau\|\tau^{\mathcal{B}}\|^2$.

From (27), if $k_v k_f \geq 0.25$, then $(v^{\mathcal{I}})^\top f^{\mathcal{I}} \leq k_v\|v^{\mathcal{I}}\|^2 + k_f\|f^{\mathcal{I}}\|^2$. Since, for $\zeta > 1$, $\zeta^t \in \mathcal{K}_\infty$, then $(v^{\mathcal{I}})^\top f^{\mathcal{I}} \leq \zeta^t k_v\|v^{\mathcal{I}}\|^2 + k_f\|f^{\mathcal{I}}\|^2 \implies h_3(x) \leq 0 \ \forall \ x \in \text{TSE(3)}$. Following the same steps, it can be verified that, for $k_\omega k_\tau \geq 0.25$, $h_4(x) \leq 0 \ \forall \ x \in$ TSE(3). Thus, $h_3(x) + h_4(x) \leq 0 \ \forall \ x \in$ TSE(3). Finally, if $k_v k_f \geq 0.25$, $k_\omega k_\tau \geq 0.25$, and since there exists a function $\alpha_\ell \in \mathcal{K}_\infty$ such that $\zeta^t(k_p\|\xi^{\mathcal{I}}\|^2 + k_R(\Psi(R_{\mathcal{B}}^{\mathcal{I}}))^2) \geq \alpha_\ell(\|\bar{x} - \bar{x}^e\|)$, then, the inequality (29) holds, and, therefore, the OCP (18) is strictly dissipative with respect to the equilibrium $(\bar{x}^e, \bar{u}^e)$.

The following theorem specifies a minimum stabilizing horizon for OCP (18).

Theorem 3. *The NMPC scheme defined by the OCP (18) is practically asymptotically stable for a sufficiently large horizon $N_p \in \mathcal{N}$.*

Proof 6. *Assumptions 1-4 are supported by Lemmas 1 and 3. Thus, according to Theorem 1, the NMPC scheme defined by the OCP (18) is practically asymptotically stable for a sufficiently large horizon $N_p \in \mathcal{N}$.*

Proposition 3. *Assuming the OCP (18) is feasible for $k = 0$ with a horizon $N_p \in \mathcal{N}$, then it is recursively feasible, i.e., it is feasible for all $k \in \mathbb{N}$.*

Proof 7. *The recursive feasibility follows from Proposition 1.*

6. Numerical Example: Quadrotor UAV

In this section, the proposed NMPC schemes are corroborated using a quadrotor UAV in numerical experiments conducted within the ProVANT simulator[2], a virtual environment based on Gazebo (Koenig & Howard, 2004) and Robot Operating System (ROS) (Quigley et al., 2009). The experiments aim to achieve point-to-point motion, guiding the vehicle from an initial configuration x_0 to a desired set-point x^e. First, the NMPC scheme (17) is tested with four different initial configurations. In the second part, the NMPC scheme (18) is evaluated using these configurations to assess not only controller efficiency but also the reduction in mission time.

6.1. Experiment setting

All experiments consider the quadrotor UAV model defined by (5)-(8), with $e^{\mathcal{B}} = e_3$ and $f_e^{\mathcal{I}} = -a_g e_3$, where $e_3 = \begin{bmatrix} 0 & 0 & 1 \end{bmatrix}^\top$ and a_g represents gravitational acceleration. To account for the limited thrust of each propeller, the following expression maps each thrust value to the input vector:

$$u = \begin{bmatrix} T \\ \tau_\phi \\ \tau_\theta \\ \tau_\psi \end{bmatrix} = \begin{bmatrix} 1 & 1 & 1 & 1 \\ 0 & l & 0 & -l \\ -l & 0 & l & 0 \\ c_{\tau f} & -c_{\tau f} & c_{\tau f} & -c_{\tau f} \end{bmatrix} \begin{bmatrix} f_1 \\ f_2 \\ f_3 \\ f_4 \end{bmatrix}, \quad (30)$$

where l is the distance from the quadrotor's center of mass to each rotor's center, and $c_{\tau f}$ is the constant determining the torque produced by each propeller. The quadrotor UAV parameters were obtained from Raffo (2011) (see Table 2.1 on page 45 for details). The controller runs at 100 Hz, with a prediction horizon of $N_p = 40$ for all results presented in

---

[2]https://github.com/Guiraffo/ProVANT-Simulator

the following subsection. The equilibrium set-point is defined as $x^e = (I_3, \begin{bmatrix} 0 & 0 & 4 \end{bmatrix}^\top, 0_{3 \times 1}, 0_{3 \times 1})$. Based on Lemmas 2 and 3, the gains for both schemes are tuned as $k_p = 150$, $k_v = 30$, $k_R = 10$, $k_1 = 10$, $k_3 = 1$, $k_\omega = 0.85$, $k_f = 5e^{-2}$, $k_\tau = 0.3$, and $\zeta = 1.2$. The initial configurations are given by $x_{01} = (R_{01}, \xi_{01}, 0_{3 \times 1}, 0_{3 \times 1})$, $x_{02} = (R_{02}, \xi_{02}, 0_{3 \times 1}, 0_{3 \times 1})$, $x_{03} = (R_{03}, \xi_{03}, 0_{3 \times 1}, 0_{3 \times 1})$, and $x_{04} = (R_{04}, \xi_{04}, 0_{3 \times 1}, 0_{3 \times 1})$, where

$$R_{01} = \begin{bmatrix} 0.1543 & 0.9880 & 0 \\ 0.1954 & -0.0305 & -0.9802 \\ -0.9685 & 0.1512 & -0.1978 \end{bmatrix}, \quad \xi_{01} = \begin{bmatrix} 4 \\ 5 \\ 7 \end{bmatrix},$$

$$R_{02} = \begin{bmatrix} -0.3045 & 0.2837 & 0.9093 \\ -0.4447 & 0.8019 & -0.3990 \\ -0.8424 & -0.5258 & -0.1180 \end{bmatrix}, \quad \xi_{02} = \begin{bmatrix} -4 \\ -5 \\ 2 \end{bmatrix},$$

$$R_{03} = \begin{bmatrix} 0.5175 & -0.3541 & -0.7790 \\ 0.8168 & 0.4755 & 0.3266 \\ 0.2548 & -0.8053 & 0.5353 \end{bmatrix}, \quad \xi_{03} = \begin{bmatrix} -4 \\ 5 \\ 7 \end{bmatrix},$$

$$R_{04} = \begin{bmatrix} 0.8660 & -0.5000 & 0 \\ -0.5000 & -0.8660 & 0 \\ 0 & 0 & -1 \end{bmatrix}, \quad \xi_{04} = \begin{bmatrix} 3 \\ -4 \\ 9 \end{bmatrix}.$$

Remark 4. *The prediction horizon N_p is chosen based on a trade-off between computational cost and control performance. For instance, controllers can be tuned with $N_p = 4$; however, a short stabilizing prediction horizon requires more conservative vehicle behavior, resulting in slower and smoother rotational and translational movements.*

The OCP solution employs the direct method introduced in Bock & Plitt (1984) to evaluate solutions for (17) and (18) at each sample time. This method parameterizes infinite-dimensional decision variables to approximate the original OCP as a finite-dimensional nonlinear program (NLP) (Rawlings et al., 2017). The direct multiple-shooting technique is used, where both piecewise control discretization and states at interval boundaries are decision variables in a finite-dimensional optimization problem. The CasADI toolbox (Andersson et al., 2018) solves this NLP, interfacing with the IPOPT solver (Wächter, 2002). The experiments are conducted on a general-purpose notebook with an Intel Core i7 4500U processor (2 physical and 4 logical cores at 1.8 GHz), 8 GB of RAM, and an NVidia GT 750M GPU, running Ubuntu Linux version 18.04.

6.2. Simulation results

Figure 1 shows the UAV trajectories during numerical experiments[3]. Both sets of experiments use the same parameter values, including gains, prediction horizon, initial conditions, and equilibrium set-point. Four distinct initial conditions are considered, including a non-equilibrium configuration, for instance, where the UAV starts upside-down initial condition x_{04}. Controllers utilizing non-singularity-free parameterization struggle with such maneuvers. Additionally, stabilizing the UAV is particularly challenging as only positive thrust values can be applied.
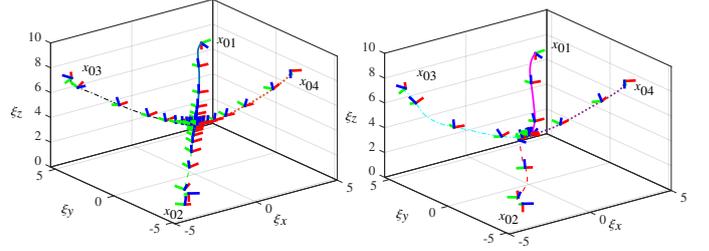

Figure 1: The UAV trajectories obtained from the experiments: the NMPC scheme (17) on the left and the NMPC scheme (18) on the right.

Figure 2 demonstrates that both NMPC schemes successfully reach the equilibrium point x^e for all initial conditions. The UAV attitude is represented using Euler angles in degrees for clarity. In all cases, the UAV attitude stabilizes at $I_3 \in \mathsf{SO}(3)$, corresponding to zero degrees for roll, pitch, and yaw angles. Notably, the UAV reaches the origin more quickly with the fast motion NMPC scheme (18), referred to as FMNMPC. Although the exponential weight in the stage cost encourages rapid stabilization of all states, the system's underactuation requires prioritizing certain states. This prioritization is achieved through the definition of controller gains. In these experiments, the faster behavior in the translational movement is evident, as the position gain, k_p, is significantly larger than the other gains. Consequently, using FMNMPC results in a considerably reduced settling time for the position vector ξ. Additionally, the vehicle exhibits more aggressive motion under the FMNMPC scheme, with larger angular excursions and higher maximum velocities.
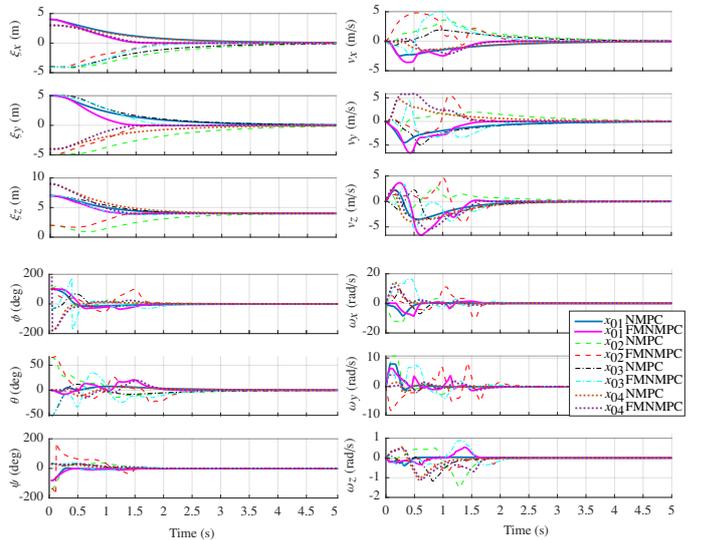

Figure 2: States trajectories of the UAV during numerical experiments.

The proposed NMPC schemes complied with all system constraints considered in the control design. Figure 3 shows the propeller forces which are mapped to the input signals, showing that the input limits, bounded between 0 and 12.3 N, are satisfied by the controllers. This demonstrates the controllers' capability to handle constrained control problems. Furthermore,

---

[3]A video of the results is available at https://youtu.be/mjKZvK4KNcY.

the FMNMPC reaches the input limits more frequently than the NMPC scheme (17), indicating its aggressiveness.
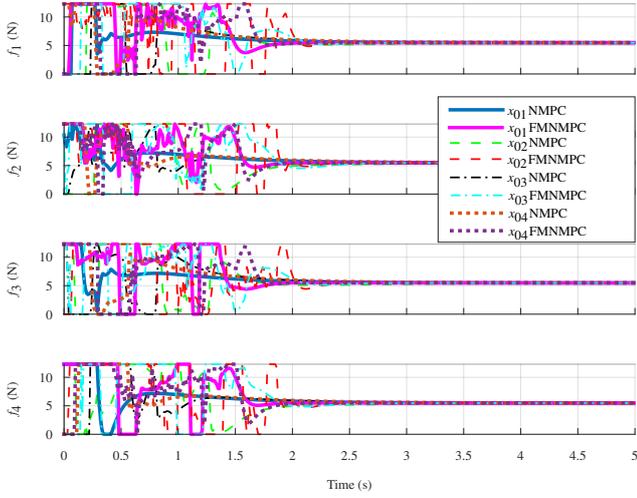

Figure 3: UAV propeller forces. The controller correctly respects the input bounds.

Lastly, Figures 4 and 5 evaluate the influence of the exponential weight on the stage cost. Figure 4 shows that the index $\|\bar{x}\|_{Q_{\bar{x}}}^2$ for FMNMPC exhibits a quicker decay in all scenarios, as expected, due to the exponential weight encouraging $\bar{x}$ to approach the equilibrium point rapidly at each prediction horizon. Additionally, Figure 5 emphasizes the faster behavior in the translational movement, with an average settling time for FMNMPC being 48% shorter, indicating a reduction in mission time. As noted in Remark 2, the parameter ζ serves as a tuning gain, allowing for adjustments in the OCP (18) to further reduce settling time with a larger ζ.
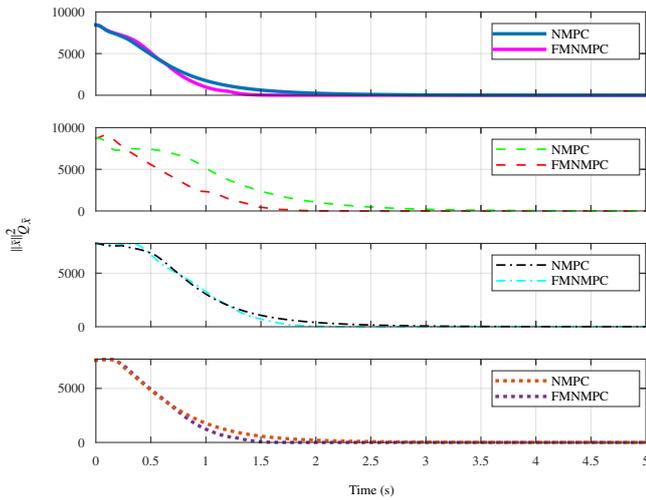

Figure 4: Variation of $\|\bar{x}\|_{Q_{\bar{x}}}^2$ for each initial condition and each proposed NMPC scheme.

7. Conclusions

This paper presented two practically asymptotically stable NMPC schemes without terminal conditions for controlling a
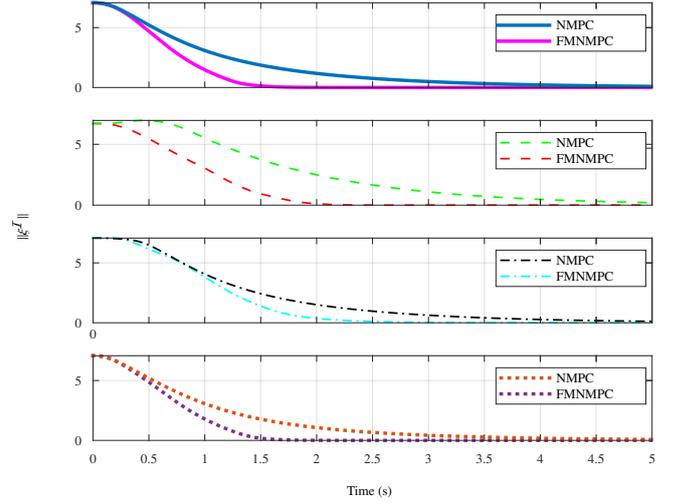

Figure 5: Variation of $\|\xi^{\mathcal{I}}\|$ for each initial condition and each proposed NMPC scheme.

class of underactuated mechanical systems with second-order nonholonomic constraints. The controllers were formulated on the SE(3) manifold, enabling a global and unique representation of vehicle motion. This singularity-free feature was evidenced in experiments where the quadrotor UAV successfully recovered from an upside-down position without additional controllers or optimization layers. The closed-loop stability and recursive feasibility were thoroughly assessed using recent theories on strict dissipativity and MPC schemes without terminal conditions. Furthermore, the proposed fast-motion NMPC scheme guided the vehicle to a desired equilibrium point while minimizing mission time as an economic criterion. Numerical experiments validated the theoretical results, showing that both controllers effectively reached the equilibrium point from various initial conditions. The analysis also explored the impact of the exponential weight on closed-loop performance, highlighting the ability to achieve a fast and stable system response with simple tuning parameters.

Future work will focus on extending the proposed NMPC schemes to address autonomous navigation in obstructed environments, integrating collision avoidance strategies, and analyzing the impact of disturbances on stability and economic criteria. Additionally, we aim to obtain experimental results by applying the proposed NMPC schemes to real-world underactuated mechanical systems.

References

Alexis, K., Nikolakopoulos, G., & Tzes, A. (2014). On trajectory tracking model predictive control of an unmanned quadrotor helicopter subject to aerodynamic disturbances. *Asian Journal of Control*, 16, 209–224.

Andersson, J. A. E., G., J., Horn, G., Rawlings, J. B., & Diehl, M. (2018). CasADi – A software framework for nonlinear optimization and optimal control. *Mathematical Programming Computation*, 11, 1–36.

Bhat, S. P., & Bernstein, D. S. (2000). A topological obstruction to continuous global stabilization of rotational motion and the unwinding phenomenon. *Systems & Control Letters*, 39, 63–70.

Bock, H., & Plitt, K. (1984). A multiple shooting algorithm for direct solution of optimal control problems. *IFAC Proceedings Volumes*, 17, 1603–1608.

9th IFAC World Congress: A Bridge Between Control Science and Technology, Budapest, Hungary, 2-6 July 1984.

Brockett, R. W. (1983). Asymptotic stability and feedback stabilization. In *Differential Geometric Control Theory* (pp. 181–191). Birkhauser.

Casau, P., Sanfelice, R. G., Cunha, R., Cabecinhas, D., & Silvestre, C. (2015). Robust global trajectory tracking for a class of underactuated vehicles. *Automatica*, *58*, 90–98.

Cenerini, J., Mehrez, M. W., woo Han, J., Jeon, S., & Melek, W. (2023). Model predictive path following control without terminal constraints for holonomic mobile robots. *Control Engineering Practice*, *132*, 105406.

Chaturvedi, N. A., Sanyal, A. K., & McClamroch, N. H. (2011). Rigid-body attitude control. *IEEE Control Systems Magazine*, *31*, 30–51.

Egeland, O., Dalsmo, M., & Sørdalen, O. (1996). Feedback control of a nonholonomic underwater vehicle with a constant desired configuration. *The International Journal of Robotics Research*, *15*, 24–35.

Eskandarpour, A., & Sharf, I. (2020). A constrained error-based MPC for path following of quadrotor with stability analysis. *Nonlinear Dynamics*, *99*, 899–918.

Ferramosca, A., Limon, D., & Camacho, E. F. (2014). Economic mpc for a changing economic criterion for linear systems. *IEEE Transactions on Automatic Control*, *59*, 2657–2667.

Fjellstad, & Fossen (1994). Quaternion feedback regulation of underwater vehicles. In *1994 Proceedings of IEEE International Conference on Control and Applications* (pp. 857–862).

Frazzoli, E., Dahleh, M., & Feron, E. (2000). Trajectory tracking control design for autonomous helicopters using a backstepping algorithm. In *American Control Conference (ACC)* (pp. 4102–4107). volume 6.

Grüne, L., & Pannek, J. (2017). *Nonlinear Model Predictive Control: Theory and Algorithms*. Springer International Publishing.

Grüne, L., Pannek, J., Seehafer, M., & Worthmann, K. (2010). Analysis of unconstrained nonlinear mpc schemes with time varying control horizon. *SIAM Journal on Control and Optimization*, *48*, 4938–4962.

Grüne, L., & Pirkelmann, S. (2020). Economic model predictive control for time-varying system: Performance and stability results. *Optimal Control Applications and Methods*, *41*, 42–64.

Grüne, L., & Stieler, M. (2014). Asymptotic stability and transient optimality of economic mpc without terminal conditions. *Journal of Process Control*, *24*, 1187–1196.

Hamrah, R., Warier, R. R., & Sanyal, A. K. (2018). Discrete-time stable tracking control of underactuated rigid body systems on SE(3). In *2018 IEEE Conference on Decision and Control (CDC)* (pp. 2932–2937).

He, X., Sun, Z., Geng, Z., & Robertsson, A. (2022). Exponential set-point stabilization of underactuated vehicles moving in three-dimensional space. *IEEE/CAA Journal of Automatica Sinica*, *9*, 270–282.

Heshmati-Alamdari, S., Nikou, A., & Dimarogonas, D. V. (2021). Robust trajectory tracking control for underactuated autonomous underwater vehicles in uncertain environments. *IEEE Transactions on Automation Science and Engineering*, *18*, 1288–1301.

Hua, M.-D., Hamel, T., Morin, P., & Samson, C. (2013). Introduction to feedback control of underactuated VTOL vehicles: A review of basic control design ideas and principles. *Control Systems, IEEE*, *33*, 61–75.

Kalman, R. E., Ho, Y.-C., & Narendra, K. S. (1963). Controllability of linear dynamical systems. *Contributions to Differential Equations*, *1*, 189–213.

Kobilarov, M. (2013). Trajectory tracking of a class of underactuated systems with external disturbances. In *2013 American Control Conference* (pp. 1044–1049).

Koenig, N., & Howard, A. (2004). Design and use paradigms for gazebo, an open-source multi-robot simulator. In *2004 IEEE/RSJ International Conference on Intelligent Robots and Systems (IROS) (IEEE Cat. No.04CH37566)* (pp. 2149–2154). volume 3.

Kunz, K., Huck, S., & Summers, T. (2013). Fast model predictive control of miniature helicopters. In *2013 European Control Conference, ECC 2013* (pp. 1377–1382).

Lee, T. (2015). Global exponential attitude tracking controls on SO(3). *IEEE Transactions on Automatic Control*, *60*, 2837–2842.

Lee, T., Leok, M., & McClamroch, N. H. (2018). *Global Formulations of Lagrangian and Hamiltonian Dynamics on Manifolds*. Springer.

Li, H., & Yan, W. (2017). Model predictive stabilization of constrained underactuated autonomous underwater vehicles with guaranteed feasibility and stability. *IEEE/ASME Transactions on Mechatronics*, *22*, 1185–1194.

Liang, H., Li, H., & Xu, D. (2021). Nonlinear model predictive trajectory

tracking control of underactuated marine vehicles: Theory and experiment. *IEEE Transactions on Industrial Electronics*, *68*, 4238–4248.

Liu, J., Jayakumar, P., Stein, J. L., & Ersal, T. (2017). Combined speed and steering control in high-speed autonomous ground vehicles for obstacle avoidance using model predictive control. *IEEE Transactions on Vehicular Technology*, *66*, 8746–8763.

Mayhew, C. G., Sanfelice, R. G., Sheng, J., Arcak, M., & Teel, A. R. (2012). Quaternion-based hybrid feedback for robust global attitude synchronization. *IEEE Transactions on Automatic Control*, *57*, 2122–2127.

Mayne, D. Q., Rawlings, J. B., Rao, C. V., & Scokaert, P. O. M. (2000). Constrained model predictive control: Stability and optimality. *Automatica*, *36*, 789–814.

Mehrez, M. W., Worthmann, K., Cenerini, J. P., Osman, M., Melek, W. W., & Jeon, S. (2020). Model predictive control without terminal constraints or costs for holonomic mobile robots. *Robotics and Autonomous Systems*, *127*, 1–12.

Murilo, A., & Lopes, R. V. (2019). Unified NMPC framework for attitude and position control for a VTOL UAV. *Proceedings of the Institution of Mechanical Engineers, Part I: Journal of Systems and Control Engineering*, *233*, 889–903.

Murray, R. M., Li, Z., & Sastry, S. S. (1994). *A Mathematical Introduction to Robotic Manipulation*. CRC Press.

Nascimento, I. B. P., Rego, B. S., Pimenta, L. C. A., & Raffo, G. V. (2023). Nmpc strategy for safe robot navigation in unknown environments using polynomial zonotopes. In *2023 62nd IEEE Conference on Decision and Control (CDC)* (pp. 7100–7105).

Nikhilraj, A., Simha, H., & Priyadarshan, H. (2019). Optimal energy trajectory generation for a quadrotor uav using geometrically exact computations on SE(3). *IEEE Control Systems Letters*, *3*, 216–221.

Ortolan, G. (2011). *Topics on geometric integration*. Università Degli Studi di Padova: PhD Thesis.

Penicka, R., & Scaramuzza, D. (2022). Minimum-time quadrotor waypoint flight in cluttered environments. *IEEE Robotics and Automation Letters*, *7*, 5719–5726.

Pettersen, K., & Egeland, O. (1999). Time-varying exponential stabilization of the position and attitude of an underactuated autonomous underwater vehicle. *IEEE Transactions on Automatic Control*, *44*, 112–115.

Pflimlin, J. M., Soueres, P., & Hamel, T. (2007). Position control of a ducted fan VTOL UAV in crosswind. *International Journal of Control*, *80*, 666–683.

Quigley, M., Conley, K., Gerkey, B., Faust, J., Foote, T., Leibs, J., Wheeler, R., & Ng, A. (2009). ROS: an open-source robot operating system. In *ICRA Workshop on Open Source Software* (pp. 1–6). volume 3.

Raffo, G. V. (2011). *Robust control strategies for a Quadrotor helicopter: an underactuated mechanical system*. Universid de Sevilha: PhD Thesis.

Raffo, G. V., Ortega, M. G., & Rubio, F. (2010). An integral predictive/nonlinear $\mathcal{H}_\infty$ control structure for a quadrotor helicopter. *Automatica*, *46*, 29–39.

Rawlings, J. B., Mayne, D. Q., & Diehl, M. (2017). *Model Predictive Control: Theory, Computation and Design*. Nob Hill Publishing, LLC, 2nd edition.

Simo, J., & Vu-Quoc, L. (1988). On the dynamics in space of rods undergoing large motions — a geometrically exact approach. *Computer Methods in Applied Mechanics and Engineering*, *66*, 125–161.

Tuna, S., Messina, M., & Teel, A. (2006). Shorter horizons for model predictive control. In *2006 American Control Conference* (p. 863–868).

Verschueren, R., Ferreau, H. J., Zanarini, A., Mercangöz, M., & Diehl, M. (2017). A stabilizing nonlinear model predictive control scheme for time-optimal point-to-point motions. In *2017 IEEE 56th Annual Conference on Decision and Control (CDC)* (pp. 2525–2530).

Wehbeh, J., & Sharf, I. (2022). An MPC formulation on SO(3) for a quadrotor with bidirectional thrust and nonlinear thrust constraints. *IEEE Robotics and Automation Letters*, *7*, 4945–4952.

Wächter, A. (2002). *An Interior Point Algorithm for Large-Scale Non linear Optimization with Applications in Process Engineering*. Carnegie Mellon University: PhD Dissertation.

Yoshimura, Y., Matsuno, T., & Hokamoto, S. (2016). Global trajectory design for position and attitude control of an underactuated satellite. *Transactions of the Japan Society for Aeronautical and Space Sciences*, *59*, 107–114.